Simulation of unsteady fluid forces on a single rod downstream of mixing grid cell

Serge Delafontaine

Simulation of unsteady fluid forces in a PWR rod bundle downstream of mixing grids

Manuscript submitted to : Nuclear Engineering and Design

***Serge Delafontaine*[1]**

[1]*French Alternative Energies and Atomic Energy Commission (CEA), DTN/STCP/LHC*

Cadarache Center, F-13108 Saint Paul Lez Durance, France

Abstract:

The present article provides an extensive analysis of the capabilities for Computational Fluid Dynamics to estimate the fluctuating fluid forces exerted by the turbulent flow with high Reynolds inside a fuel rod bundle with mixing grids. It benefits from high accuracy experimental results obtained through an original device developed at CEA and providing a direct measurement of the fluctuating pressure on the surface of the rods, allowing the characterization of the turbulence scales and effects close to walls and therefore representing a valuable reference for the qualification of turbulence models. To perform in-depth comparisons between state-of-the-art numerical models (implementing either Unsteady-RANS or LES), a first intermediate configuration implementing one single rod and one grid equipped with mixing vanes is considered. It shall be followed by advanced analyses in bundle configurations with numerical models following the conclusion proposed hereby.

Keywords: Pressurized Water Reactor (PWR) , Fluid-structure interaction, Fuel rod vibrations, Grid to rod fretting wear, Turbulent flow, Computational Fluid Dynamics (CFD).

1. Introduction

Pressurized water streaming at high speeds (order of 5 m/s) is used as a coolant in the fuel assemblies of PWR nuclear reactor cores. Each fuel assembly is made of a four meters height bundle of rods containing the nuclear fuel. The main structure of the assembly is composed of vertical guide tubes equipped with regurlarly spaced grids, ensuring the mechanical support of the rods through a spring and dimple system allowing distension due to thermal constraints.

In assemblies, fluid flow is mainly axial, and thus, additionally to their structural role, grids have a temperature homogenization role in order to avoid hot points. This function is guaranteed by mixing vanes implanted on the downstream side of the grid cells, generating turbulence and flow redistribution between hydraulic sub-canals of the rod bundle.

Burn-up rate improvement of the fuel leads assemblies to spend more time inside the core. Relaxation of springs can favor the rise of the vibratory level of the rods which are subjected to the fluid turbulence excitation.

Those vibrations are the source of fretting, *i.e.* the wear under small vibratory movements at the contact points of the rods with the springs and the dimples in the grid cells. In some extreme cases,

this may lead to the piercing cladding of the fuel rod, the first confinement barrier, with a consequential dispersion of fission products in the primary circuit.

Carried out at the *Laboratoty of Core and systems Hydrodynamics* (abbreviated *LHC* in the rest of the paper) in CEA Cadarache, the research program involving the current contribution comprises two parts and its purpose is the determination of the vibratory excitation forces. Those are due to the fluctuating pressure fields on the surface of the rods of PWR fuel assemblies, in particular downstream of retaining grids.

- The experimental part concerns the study of the flow in mockups of 5x5 rod bundles with hydraulic reference configurations. Classical measures through vibrometry and laser velocimetry are combined with new measurement system of the pressure fluctuations directly on the wall of the rods, which was developed at LHC [1].
- The second part aims at validating the CFD simulation methods that estimate the fluctuating fluid forces exerted on rod bundles at high Reynolds. One of the ultimate objectives is to get a set of qualified tools and computation methods to calculate the excitation forces. The other one is to improve the understanding of hydraulic phenomena in areas that are less accessible to measures.

A precise determination of the vibratory excitation spectra is used as input for the computation of the vibratory behavior of the rods under turbulent flow using a non-linear vibratory mechanics code [2-3]. It is secondly relevant to compare the computational results to measures of the rods dynamics obtained by vibrometry, like those obtained from the full scale "Hermès" test loop hosted at the laboratory.

The general aim of that program is thus to improve the design of the fuel assemblies to guarantee the integrity of the first safety barrier and to limit the maintenance operations on the PWR reactors and to improve the plant availability rate.

In this context, the present article focuses on the characteristics of the CFD simulation techniques necessary to correlate the fluctuating pressure measurement, especially in terms of turbulence models and mesh sensitivity. Directly adressing the 5x5 bundle configuration would lead to very large computational models (around 200 millions fluid cells for a standard accuracy) and would not be compatible with the test of multiple parameter combinations as it is expected in this phase. A preliminary implementation of the fluctuating pressure measurement device is therefore chosen for simulation/experience comparisons. The geometry is representative of the main issue, but with only one rod, making it more appropriate for mesh sensitity analyses, with models from 7 to 15 millions cells, and tests of many turbulence models.

2. Benchmark experience and computational models

2.1 Single rod test loop

The single rod mockup, equipped with one grid cell and used for preliminary validation of the new measurement system of the parietal pressure, is described in Figure 1.

Upstream and downstream of the grid cell, the flow develops in an annular space between the cylindrical confinement and the instrumented rod. The grid cell with mixing vanes has been included in the test bed to get turbulences that was representative of those studied in the 5x5 experimental facilities. The specific features of the fluctuant pressure measuring system and the synthesis of main most significant results are presented in Francis Moreno's article [1].

In each of the studied cases, we consider the turbulent and isotherm flow of an incompressible fluid in steady state. The selected parameters for the modelization are as follows:

- Test fluid: water (monophasic) Flow rate: 3 m/s

- Fluid temperature: 20°C Pressure: 1,244 bar
- Density : ρ= f(P,T): 998,217 kg/m3 Dynamic viscosity: μ= f(P,T) : 1,0016.10-3 Pays
- Reynolds (current section): 87902

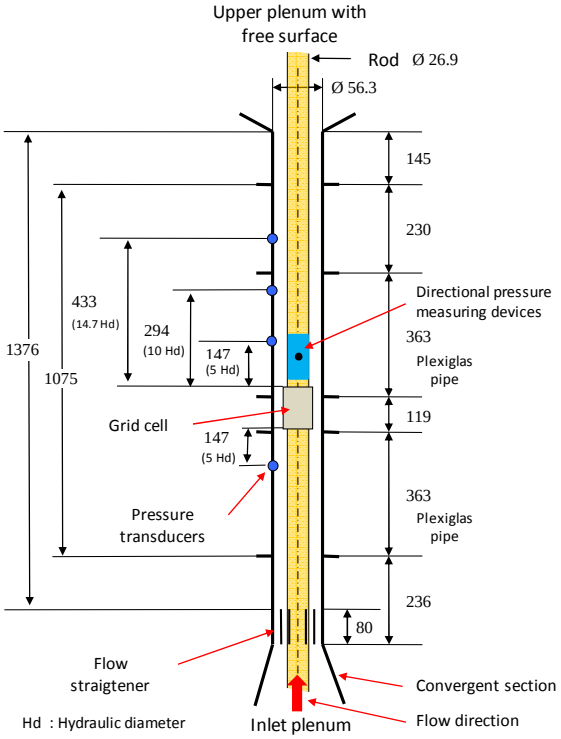

Figure 1 : Schematic and photography of single rod experimental setup

2.2 Modeled geometry

The modeled geometry focuses on the pressure fluctuation area in the range of 1.7 H_d to 14 H_d respectively upstream and downstream of the grid (see Figure 2).

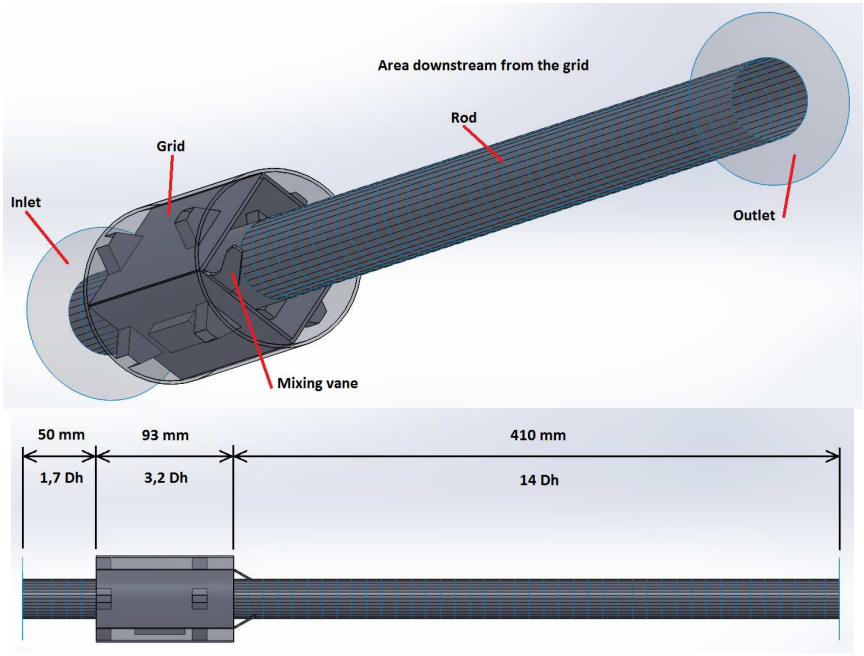

Figure 2 : Geometry details

The geometry of the fluid domain is developed using the CAD software *SolidWorks*. Simplifications of external volume of pieces are necessary to:

- remove details such as threaded holes receiving mounting screws,
- remove welding points producing a pressure losses in the range of 1-2%
- create fillet radius on the surface contact of rods with springs or dimples to avoid points of tangency with angles lower than 10°.

2.3 Mesh generation - Quality criteria

The different meshes of the domain are designed with Ansys ICEM-CFD software. Tetrahedrons elements are used to match the requirements from TrioCFD software [4], used for all the simulations.

To correctly solve the Navier-Stokes equations within the fluid domain at high Reynolds turbulent flows, the mesh should address strong and contradictory constraints. It involves depicting the geometry as faithfully as possible and setting a minimum number of discretization points (15 to 20) between opposite faces while controlling the minimal size of the cells.

In turbulent flows at high Reynolds, the speed profile to the wall is very steep. A complete description of the boundary layer would lead to mesh sizes with y^+ close to 1, yielding a too large computation time, so that an established analytical law is prefered to reproduce the behavior of the fluid close to the wall. With URANS modelling, the first mesh point must be placed instead in the logarithmic layer (practically in the range $32 < y+ < 400$). For LES modeling, particularly with the WALE model (see Section 2.5 for details), there is no condition for locating the first mesh point. We also chose $y+ > 30$ anyway, but the reason is then to limit the number of elements in the meshes and to control the minimum time steps.

In the case of stagnation point (e.g. impact on a wall) or of point of separation of the flow at the wall, the use of a wall law may give poor results. Such patterns are found in the perimeter of the grid, but a fine mesh of the boundary layer associated with fluid velocities greater than 6 m/s within the grid, due to the restriction of the cross-section, would lead to calculation time steps of less than 1.10^{-7} s, consequently compromises are necessary to reach the turbulent regime established over the whole domain in an acceptable calculation duration.

Fortunately, the use of a wall law is well adapted in the case of established flow when the boundary layer is in equilibrium, which is the case in the zones along the rod located upstream and downstream of the grid, where measurements of pressure fluctuations at the wall of the rod are made. The Reichardt law [5] correctly reproduces the dimensionless velocity profile for $y^+ < 4$ and $y^+ > 32$ and ensures the transition in the buffer zone. This law, valid in three zones of the boundary layer in a wide range beyond $y^+ > 500$ (see Figure 3), is seen as the most suitable in the present situation.

$$U^+ = f(y^+) = \frac{1}{\kappa} ln(1 + \kappa y^+) + 7.8\left(1 - e^{-\frac{y^+}{11}} - \frac{y^+}{11} e^{-0.33y^+}\right)$$

With: $U^+ = \frac{1}{\kappa} log(y^+) + C$

$\kappa = 0{,}415$ Von Karman constant

$C = 5.32$ or $C = 5.5$ (Nikuradse).

$U^+ = \frac{U}{u^*}$ Dimensionless velocity

$u^* = \sqrt{\frac{\tau_p}{\rho}}$ Friction velocity with: τ_p: Wall shear stress

$y^+ = \frac{y}{y^*}$ Dimensionless wall distance with: $y^* = \frac{\nu}{u^*}$.

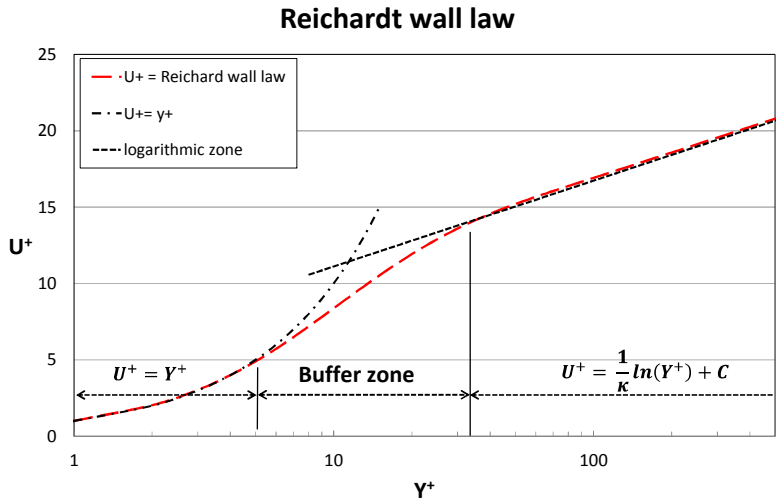

Figure 3 : Comparison of Reichardt law with the boundary layer properties

2.4 Generation of the flow profile at the inlet of main domain

A periodic box (see Figure 4) is used to generate, on the inlet of the computational domain, a velocity profile and a turbulent intensity representative of the cross-section of the flow. This secondary domain is constructed by extrusion of the mesh of the inlet face of the main domain. In each case, we use the same turbulence model and the same numerical schemes than those used in the main domain.

At each time step the output profile of the periodic box is simultaneously applied as an initial condition at the inlet of the main study domain and reinjected at the inlet of the periodic box to calculate new initial conditions at the next time step. To compensate the pressure drop of the periodic box, the pressure gradient is corrected at each time step in order to maintain the flow rate injected at the main inlet.

For URANS simulations, a box length of the order of 1.5 to 2 H_d is sufficient not to auto-correlate the turbulent fluctuations between the output and the input, which can generate unrealistic pulsating phenomena at the inlet of the main domain. For Large Eddy Simulations (LES), 8 to 10 H_d is necessary to overcome these disadvantages.

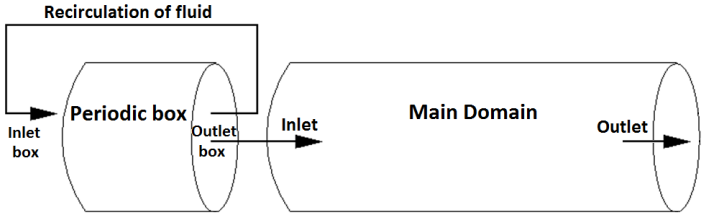

Figure 4 : Operating principle of a periodic box

2.5 Turbulence models and numerical schemes

Two classes of models available in TrioCFD are more suited to the study of unsteady flows in complex geometries. The present article proposes a systematic review of the different models to define which approach is the most adapted to the topology of the flow specific to our configuration.

- Unsteady model URANS (k-ε)

The URANS unsteady model [5], widely used in the industrial field, has many advantages, starting with its computational efficiency, as well as some weaknesses. The turbulent kinetic energy is overestimated in impact and attachment regions, while recirculations in swirl flow are underesti-

mated. This is mainly due to the diffuse nature of the model, which represents the Reynolds tensor in the form of a diffusive term. The reattachment after fluid detachment is generally wrongly predicted. Some flow patterns of this kind are present in our geometry due centering pads, dimples and mixing vanes.

Unsteady URANS models do not require a high order numeric time schemes, several schemes can be used. For the URANS simulations, the explicit Euler scheme associated with the iterative linear GMRES (Generalized Minimal Residual Method) with a convergence threshold of 1.10^{-6}, gave the best compromise between stability and speed of computation.

In the finite volume element discretization implemented in TrioCFD to solve scalar convection-diffusion equations and momentum Navier-Stockes equations, the second order TVD scheme EF_stab (see Kuzmin and Turek [8]) is the best adapted scheme [4]. Computational convergence is ensured by weighting the centered convection EF_Stab scheme with an upwind scheme through an alpha factor taken between 0 (full centered scheme) and 1 (full upwind scheme). This α factor allows to find a compromise between robustness and diffusive features. EF_Stab with α=1 is stable but diffusive and it generally gives average results when the forced convection flow has a preferred direction, as it is the case like in bundle of rods. On the contrary, EF_Stab with α= 0.2 is known to give better results and it is required in complex geometry (like grid area). It is less diffusive but also less stable.

The main characterics of the implemented URANS models are given in Table 2, where 3 different meshes are considered and described in Section 2.6.

Table 1 : URANS model parameters (k, ε)

Meshing	Tetrahedrons	At least 15 to 20 calculation points in annular space between the rod and tube
Discretization	Finite Element Volumes	P0/P1 for the pressure (P1NC/P1 Bubble elements) P1NC non-conform for velocity
Time scheme	Explicit	1er order Euler backward
Momentum transport	Convection	- Upwind scheme for periodic box - 2nd order EF-Stab (mixed centered and upwind) with low stabilization (with α=0,3)
	Diffusion	2nd order centered
	Wall treatment	Reichardt law : $y^+ > 32$
	Turbulence	K- ε model with standard coefficient with temporally correction of local high value of turbulent viscosity during transient
Numerical solver	Implicit	GMRES solver
Time steps	Box +Domain : URANS 1 : 5,3 10^{-6} s; URANS 2 : 3,5 10^{-6}s ; URANS 3 : 2,4 10^{-6}s	
Physical time calculated	Box alone before coupling : 1 s Box + Domain : URANS 1 : 0,8 s ; URANS 2 : 1 s ; URANS 3 : 1 s	

Our geometry exhibits two zones with opposite properties, a regular geometry for the rod and the zone of the grid with obstacles and sudden contraction of flow. At the beginning of the simultation, before the transition to turbulence (between 0 and 0.25 seconds), the calculation is thus started with medium stabilization (α = 0.5), and α is reduced up to 0.3 after. The value α= 0.2 does not fit due to numerical instabilities causing divergence.

Achieved physical computation times in the range 0.8 to 1 s are such that fluid can travel the domain at least five times. Transition to turbulence is complete all over the domain at approximately

0.25 s, this leaves sufficient time for post-processing pressure fluctuation in temporal and frequency domains.

- Unsteady model LES (WALE)

The WALE (Wall Adapting Local Eddy-Viscosity) model [6] is based on the Smagorinsky approach [7-8] for which the characteristic time scale of the mesh scales is constructed with both, the tensor of deformation $\tilde{S}_{ij}$ and the tensor of rotation $\tilde{\Omega}_{ij}$. This new approach makes it possible to take into account the turbulent regions where the vorticity is greater than the deformation rate and to provide a good behavior of the turbulent viscosity, tending towards zero at the wall with the correct diminishing rate ($\sim y^3$), without using damping function to reproduce the no-slip boundary. Moreover the model predicts the laminar turbulent transition.

LES (large eddy simulation) models need adapted numerical schemes. For explicit time integration scheme, LES require high order schemes. The 3rd-order Runge Kutta scheme thus appears as a good compromise between the speed and the accuracy of solution and it retains the kinetic energy [13]. Regarding the convection scheme in the VEF (finite volume element) discretization, LES WALE simulation require a second order TVD scheme EF_stab for solving the scalar convection-diffusion equations and the momentum Navier-Stockes equations [4].

In the same way of the previous URANS simulation, the computation convergence of the centered numerical scheme was weighted by an upwind scheme to ensure a better stabilization (for periodic box calculation $\alpha = 0.4$ and for the domain calculation $\alpha = 0.3$). In these cases lower alpha values provide numerical instabilities.

The main characterics of the implemented LES WALE models are given in Table 3, where 2 different meshes are considered and described again in Section 2.6.

Table 2 : LES (WALE) model parameters

Meshing	Tetrahedrons	At least 15 to 20 calculation points in annular space between the rod and tube
Discretization	Finite Element Volumes	P0/P1 for the pressure (P1NC/P1 Bubble elements) P1NC non-conform for velocity
Time scheme	Explicit	3rd order Runge-Kutta
Momentum transport	Convection	- Periodic box : 2nd order EF_stab (mixed centered and upwind) with low stabilization (with α=0,4) - Domain : 2nd order EF_stab (mixed centered and upwind) with low stabilization (with α=0,3)
	Diffusion	2nd order centered
	Wall treatment	Reichardt law : no condition on y^+ thickness
	Turbulence	LES Wale model with temporally correction of local high value of turbulent viscosity during transient
Numerical solver	Implicit	Petsc Cholesky solver
Time steps	Box +Domain :	WALE 1 : 2,6 10^{-6} s; WALE 2 : 2,3 10^{-6} s
Physical time calculated	Box alone before coupling : WALE 1 : 2,3 s ; WALE 2 : 2,0 s Box + Domain :	WALE 1 : 2,0 s ; URANS 2 : 2,0 s

The simulated physical time is set to 2 seconds in this case, which lets the fluid travel at least eleven times the studied domain. Moreover, the stabilization of the values is achieved (transient not included) for the different probes placed all over the domain and it allows a sufficient duration for the post-treatment in both time and frequency domains.

Remarks on the Unsteady LES Smagorinsky-Lilly model

The Smagorinsky-Lilly turbulence model [10] has been tested on the same meshes of the periodic boxes than those used with the LES WALE models (1 and 2). In both cases, no transition to turbulence is observed after 0.3s of computation time.

By initializing the obtained velocity fields achieved with the previous LES WALE models in established turbulent flow and by computing LES Smagorinsky-Lilly, we observe a rapid return from the turbulent regime to a mean flow without any fluctuation. This model is consequently not suited for both geometry and flow conditions of the annular channel.

Dynamic LES Smagorinsky models (variation of Smagorinsky-Lilly model) could not be tested since they are not available in TrioCFD.

2.6 Mesh Configurations

Four meshes of the domain were realized for the five calculation configurations (3 for URANS and 2 for LES WALE). Some meshing details are given in Figures 5(a) and 5(b). The various mesh and calculation configurations are summarized in Table 1. The first two URANS models have a y^+ value of 58 and 50, respectively 0.3 mm and 0.25 mm thick of first mesh layer.

The mesh of the third URANS modelization with a y^+ of 50 is more refined inside the grid. The fourth modeling uses the previous mesh but this time with a LES turbulence model. The last mesh used for the second LES calculation has a value of y^+ at the wall of 32 or 0.15 mm of thickness of the first meshing

Table 3 : Main characteristics of the studied mesh

Models	**Meshing parameters**			**Domain**	**Periodic box**
	Domain **Maximum size in mm and Growth ratio mesh**	**Y^+**	**Wall** **Number of layers / thicknesses in mm**	**Nb. Tetrahedrons / Nb. processors**	**Length / Nb. Tetrahedrons / Nb. processors**
URANS 1	1,2 / 1,2	58	3 / (0,3 | 0,36 | 0,432)	7.737.673 / 352	1 H_d / 540.480 / 26
URANS 2	1.1 et 1,2 / 1,2	58	3 / (0,3 | 0,36 | 0,432)	8.242.119 / 448	1,5 H_d / 829.500 / 40
URANS 3	1,1 /1,2	50	3 / (0,25 | 0,3 | 0,36)	8.690.825 / 448	2 H_d / 1.722.000 / 80
LES WALE 1	1, 1 /1,2	50	3 / (0,25 | 0,3 | 0,36)	8.690.825 / 448	8 H_d / 6.888.000 / 336
LES WALE 2	0,9 / 1,1 et 1,2	32	3 / (0,15 | 0,195 | 0,254)	14.667.867 / 496	8 H_d / 12.619.864 / 496

The optimization efforts on the meshes mainly focus on compliance with the general criteria related to the minimization of numerical errors while respecting growth ratios of maximum size varies from 1.1 to 1.2 between two neighboring meshes. Throughout the domain, the ratio between the maximum and minimum mesh volumes must not be greater than 1000. Particularly in the case of the LES models, the aim is to get a range of vortex sizes representative of the frequency content of the turbulent flow, and to respect the characteristically propagation times of the convection phenomena of the turbulence and diffusion related to the viscosity.

The control of the criteria on the maximum and minimum angles (mesh distortion) and on mesh elongation makes it possible to avoid the propagation of numerical calculation error.

The quality of the different meshes is checked by comparison with results of publications [6-7] for the periodic boxes and with the experimental results obtained in the laboratory [1].

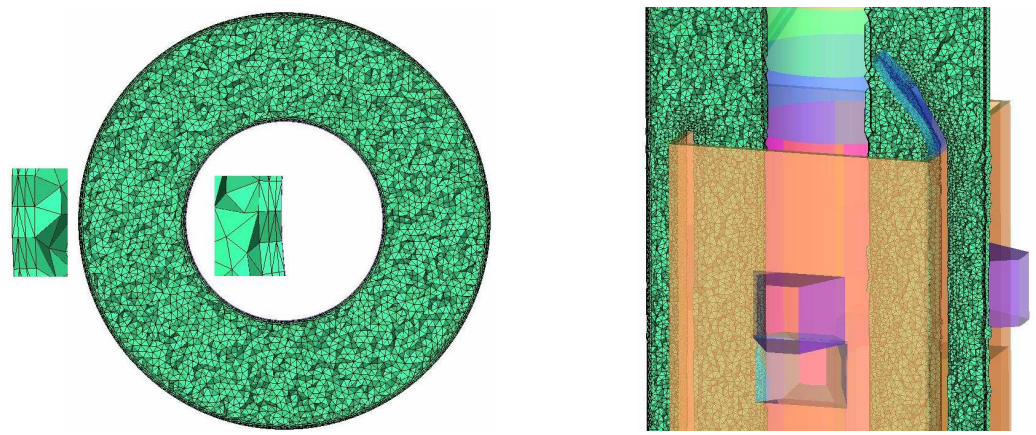

(a) Cut in the current section and boundary layer wall (b) Vertical cut section in the grid

Figure 5 : Details of the mesh of LES WALE 2model

2.7 Boundaries conditions

The modeling consists of two associated domains: the recirculation box (whose role has just been presented) and the main computational domain. The boundary conditions are as follows.

- For the periodic box:
  - Periodic input and output sides: imposed flow rate with a source term to conserve the moment
  - Speed condition: 3 m/s
  - Pressure condition: Free inlet and outlet pressure.
  - Wall condition: No-slip conditions for central rod and outer pipe.
- For the main domain:
  - Non-periodic input and output sides;
  - Pressure condition: Free inlet pressure and not fixed at the outlet.
  - Speed condition: At each time step, the speed profile imposed at the input of the main domain is equal to the output speed profile of the periodic box.
  - Wall condition: No-slip conditions for central rod, external pipe and grid.

2.8 Signal processing probes

Probes are identically arranged for all simulations, located at the same axial and azimuthal co-ordinates as the measurements of the parietal pressure sensor. Comparing the results of each model with the corresponding measurements allows a detailed analysis of the reproduction of the forces at the wall along the rod.

The probes for local evaluation of the pressure fluctuations are placed every 10° round the perimeter of the rod on 6 planes located at: 1, 2, 2.33, 3, 4 and 5 H_d from the grid top edge.

The evaluation of the pressure resultant is calculated on 41 rings of identical height ($H_d/3$) along the central rod. The three components of the pressure forces F_p and the three components of the shearing forces F_τ are spatially integrated on each ring to determine the resultant of the pressure forces in the transverse plane XY per unit area and the resultant of shear forces per unit area along the longitudinal axis Z.

Samples of the pressure fluctuation signals are selected after the transition to turbulence, when the ergodicity criterion is reached. Analysis and comparisons of the signals of the probes make use of classical functions of signal processing [14]. Data processing and plotting of the curves were realized with *Matlab* software [15].

The signals are analyzed in the frequency domain. The PSD (Power Spectral Density) gives the energy distribution of a signal as a function of the frequency. The calculation of the PSD is ob-

tained from the discrete Fourier transform S(k) through :

$$PSD(k) = \frac{1}{N}.\|S(k)\|^2 \qquad \text{with :} \quad S(k) = \frac{1}{N}\sum_{n=0}^{N-1} s(n.T_e).e^{-2.\pi.j.n.k/N}$$

N : number of samples, n : current sample, T_e : sampling time, $s(n.T_e)$: discretized signal.

The analysis FIX vibration tests [13], induced by turbulent flows in rods bundle or in internal flows J. M. Clinch [14], led to the establishment of reference spectra. Adimensioning these spectra, allows comparisons on a common basis of results from different experiments, over a wide range of Reynolds by adopting the following scaling factors:

$P_{ref} = \rho_0.V_0^2,\ f_{ref} = \frac{V_0}{D}$ with : ρ_0 : fluid density, V_0 : flow rate velocity, D : rod diameter

The dimensionless PSD : $S_{ad}(x,\theta,f_r)$ is linked to the physical PSD $S(x,\theta,f)$ in $Pa^2.Hz^{-1}$ by the relation : $S_{ad}(x,\theta,f_r) = \frac{S(x,\theta,f)}{\rho_0^2.V_0^3.D}$ with reduced frequency : $f_r = \frac{f.D}{V_0}$ and V_0: bulk velocity

Our single-rod test bench has hybrid characteristics between a flow around a rod equipped with a grid and an internal flow in a circular pipe; we use as a basis of comparison two types of dimensionless spectrums :

- PSD wall pressure spectrum of axial flow inside rod bundles FIX [13] (see figure 6(a)), they are of the form : $\Phi_{f_e}^a(f_r^a) = a.f_r^{-p}$, with a change of slope at the reduced frequency located at $f_r = 0.2$
  $\Phi_{f_e}^a(f_r^a) = 2\times10^{-6}.f_r^{-0.5}$ for : $f_r \le 0.2$ et $\Phi_{f_e}^a(f_r^a) = 1.5\times10^{-8}.f_r^{-3.5}$ for : $f_r \ge 0.2$
- PSD wall pressure spectrum of axial flow inside, at the internal wall of cylindrical pipe Clinch [14], they are also of the form : $\Phi_{f_e}^a(f_r^a) = a.f_r^{-p}$, with three different slopes. A first slope to power -1/4 for : $f_r \le 1$, a second slope to power -5/3 for : $1 \le f_r \le 10$ and a third slope to power -9/2 for : $f_r \ge 10$ (see figure 6(b)).

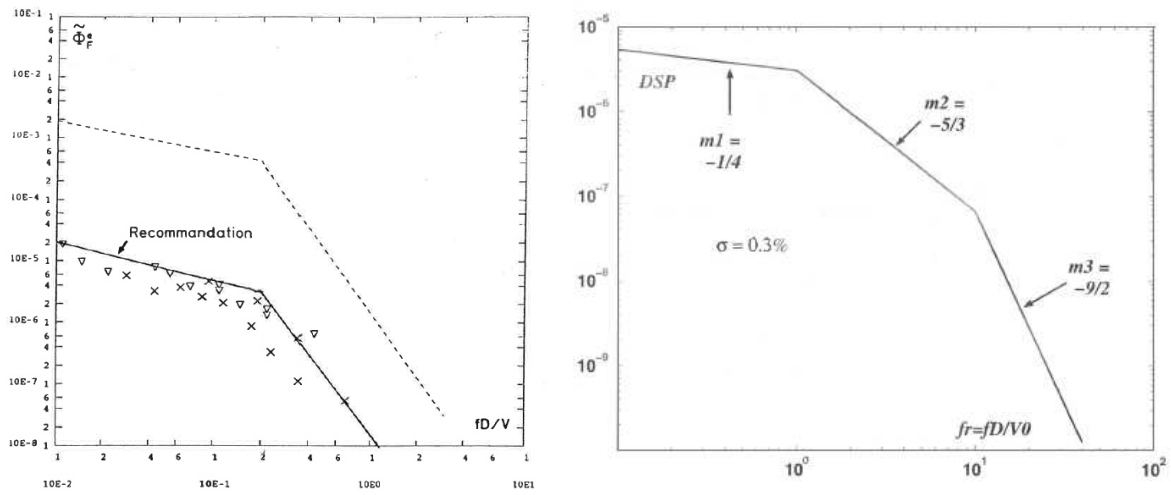

(a) FIX spectrum *(b) Clinch and Axisa spectrum*

Figure 6 : Dimensionless reference PSD spectrum

3. Computational results and comparison methodology

In this section, the analysis of simulation results is provided along six topics.

First, the flow in the recirculation box, representative of an unobstructed flow in annular section, can be compared with the results of the experimental work of JM Nouri (et al.) [16] and the DNS simulations of SY Chung (et al.) [17].

Then, the results of the five simulations are compared with the Moreno experimental data [5]

and [6]: the comparisons concern the azimuthal distribution of pressure fluctuations at the rod wall in different planes spaced after the mixing grid and local measurements of the spectral power densities.

The topology of the flows in the fluid domain is succinctly presented because the single-rod test bench does not allow measurements of velocity fields by LDV laser velocimetry. However the presented visualizations of the streamlines and the cross sections of axial and transverse velocities in different planes, shed light on the distribution of observed pressure fluctuations. Finally, the computations of the resultant pressure forces integrated onto the wall of the different models will be compared with the data of the literature [18] and [19].

These cross-comparisons, although partial, gives us a first insight to discriminate between models on the basis of qualitative criteria derived from the literature and more objective criteria derived from the experimental results.

3.1 Mean velocity profile in recirculation boxes

The works of Nouri (and al.) [16] and Chung (and al.) [17] deal with flows in concentric annular spaces. The experiments and calculations are performed in turbulent flow (Re = 8900) with a ratio between the inner radius on the outer radius, α = 0.5. This work gives the mean velocity profiles normalized with respect to the flow velocity and plotted as a function of the dimensionless distance between the walls, we note : $2.\delta = R_{outer} - R_{inner}$. In our geometry α = 0,478 is very close to the reference. The flow is turbulent, but in our case the Reynolds number of 87902 for a velocity flow rate of 3 m / s in the section is higher.

It is observed that the five models (see Figure 7) give very close results in the central part. They are between the measurements of Nouri and the recalculated values from the Chung model and the LES WALE 2 model is the closest to the values of Chung.

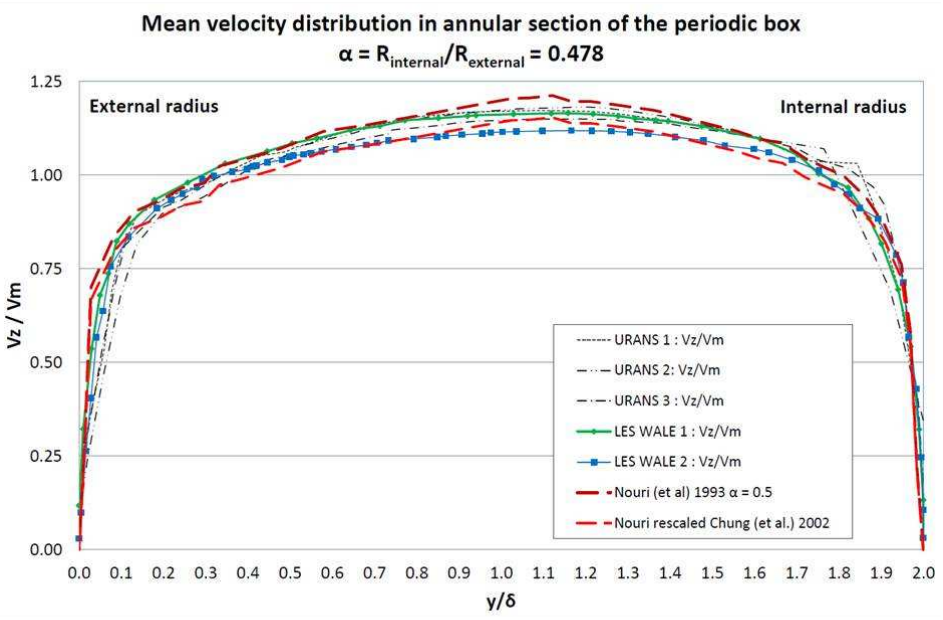

Figure 7 : Velocity profile in the annular section

In the zone near the wall of the outer radius (δ ≈ 0), the two models LES WALE 1 & 2 are those which have the profiles closest to those of Nouri and Chung. The profiles of the URANS 1 & 2 models are very steep and not very detailed near the outer wall. We note the influence of the choice of turbulence model between the cases URANS 3 and LES WALE 1 which share the same mesh and the same wall law, the LES modelization gives a profile of speed more in conformity with the references profiles.

In the zone near the wall of the inner radius ($\delta \approx 2$), the LES WALE 1 & 2 models are again the closest to the values of Nouri and Chung, with a better resolution of the WALE 2 model. The three URANS models are much less resolved near the inner wall. Here again, as near the outer radius, we note the best resolution of the LES WALE 1 model on the URANS 3 model using the same mesh.

It is noticeable that these profiles are reproducible over the entire circumference of the section in different horizontal planes along the vertical direction of the box.

The measurements in the computational domain closest to the configuration of the barrier-free periodic box correspond to the zones of the loop located in the plane 5 H_d upstream of the mixing grid. Averaging the experimental pressure fluctuations over the 36 azimuthal measurement points spaced every 10° in the -5 H_d plane before the grid gives a reproducible value of 53 Pa over a period of 100 s. The model LES WALE 2 gives an average value of pressure fluctuations at the wall of 51.3 Pa, representing an accuracy of 3.2% with the measurements. This value is calculated from the mean of the standard deviation over the 72 pressure probes arranged every 5° in the plane located at 1 H_d before the output of the box over a period of 2 s.

As a first conclusion, we find that the turbulence model LES in the case WALE 2 with a y^+ of 32 to the wall is the one which has the most averaged mean velocity profile with respect to the measure and the literature. It should be added that the use of the periodic boxes is well adapted to the generation of turbulent unsteady profiles at the inlet.

3.2 Comparison of simulation results with measurements in the main domain

- **Azimuthal pressure fluctuations at different altitudes**

The first topic of comparison concerns the spatial distribution and the amplitude of the pressure fluctuations at the azimuthal probes located on the rod wall for different altitudes.

- **Measurements of fluctuations of azimuthal pressures at the wall**

At the level -5 H_d upstream of the grid, the measurements, carried out every 10° at different altitudes, show a uniform distribution of the uniform pressure fluctuations over the entire circumference (see Figure 8). The mean amplitude of the fluctuations calculated over all the probes is 53 Pa. At the distance 1 H_d downstream of the grid, the azimuthal distribution of the pressure fluctuations is strongly influenced by the eddies in the wake of the mixing vanes and by the jet effects at the grid outlet. These phenomena induce significant differences in amplitudes according to the angular position. The maximum amplitudes are 500 Pa and 550 Pa in the wake of the fins respectively for the angles of 40° and 220°, secondary maxima are observed at 160° and 310°. At level 2 H_d downstream of the grid, the distribution is less irregular, the mean fluctuations are around 200 Pa, and there are two maximums at 290 Pa (azimuth 50°) and 250 Pa (azimuth 220°). The angular offset of the maximums is about 10° compared to the level 1 D_h. At +3 D_h downstream of the grid the maximum amplitudes are 160 Pa and 220 Pa, the angular offset compared to the previous level is between 5° and 10°. At 5 H_d level, the maximum amplitude is about 110 Pa, the distribution of the fluctuations is almost circular again.

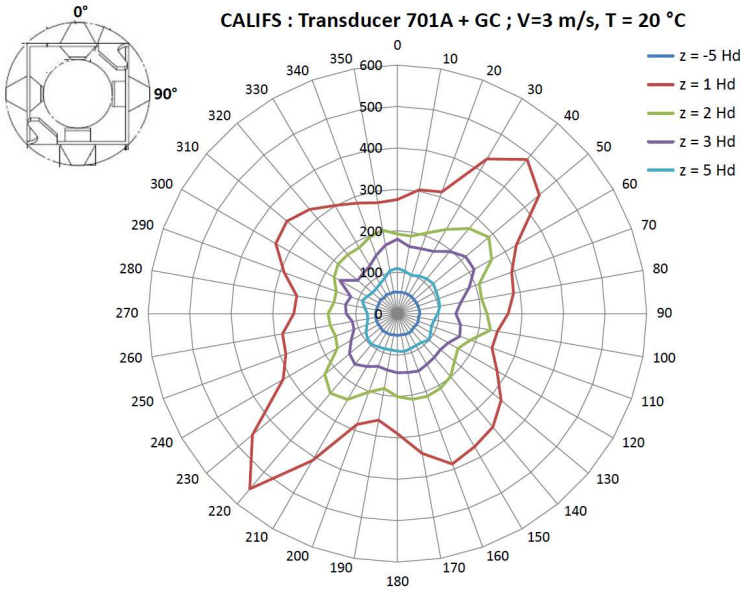

Figure 8 : Fluctuation pressure profiles at different levels

- **Fluctuations of simulated azimuthal pressures**

In the simulation results presented in Figures 9 to 13, the azimuthal digital probes are spaced at 5° with a positioning accuracy of ± 0.3 °.

The first URANS 1 model (Figure 9) gives globally larger fluctuations than the measurements at altitude 1 H_d. But for the following levels, the values of the maximum fluctuations are underestimated by about 30%. The dissipation is globally faster than in the experiment and the angular orientation of the maxima is not reproduced correctly by this model.

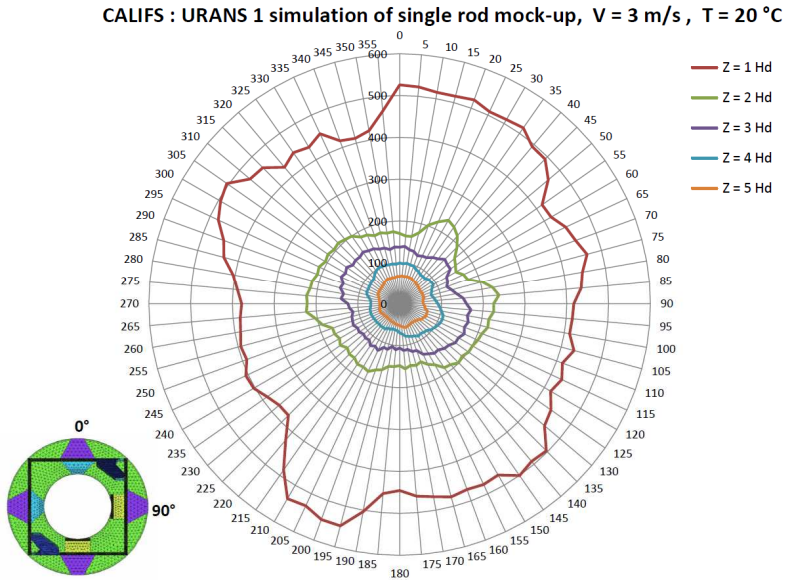

Figure 9 : URANS 1 - Azimuthal fluctuations pressure at different levels

With the URANS 2 model (Figure 10) the maximum amplitudes are 500 to 550 Pa in the wake of the fins at altitude 1 H_d, which is comparable to the experimental values. For the following levels 2 H_d and 3 H_d the values of the maximum fluctuations are underestimated by approximately 20% to 25%. At the distance of 5 H_d the levels are correct. In all planes the angular orientation of the maxima is not correctly reproduced by this model.

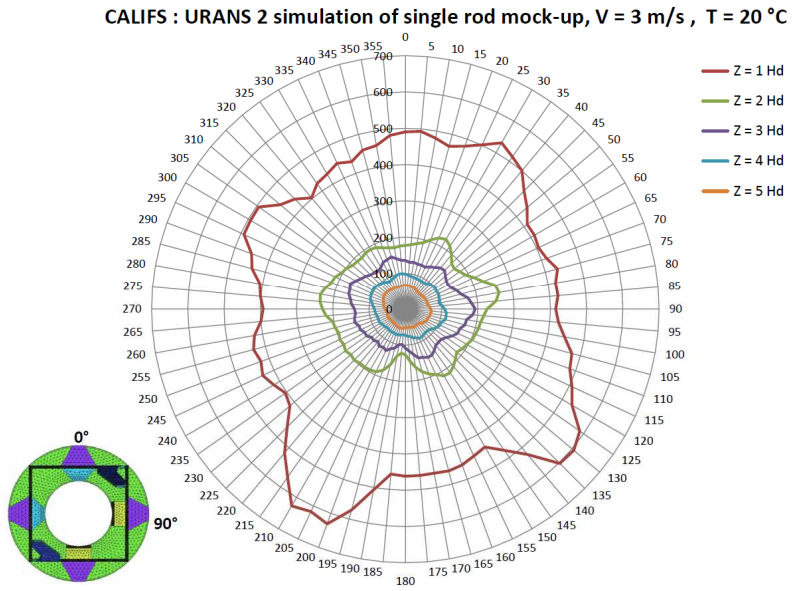

Figure 10 - URANS 2 - Azimuthal fluctuations pressure at different levels

The following model URANS 3 (Figure 11) gives correct fluctuation levels at altitude 1 H_d. The amplitude maxima of 530 Pa in the wake of the fins approximate the experimental values. They are oriented at 35° and 210° and are less angularly spread out than in the two previous models. For the following levels 2 H_d and 3 H_d the values of the maximum fluctuations are underestimated by approximately 30% to 40%. At 5 H_d, the level is correct. The angular orientation of the maxima is again not correctly reproduced here.

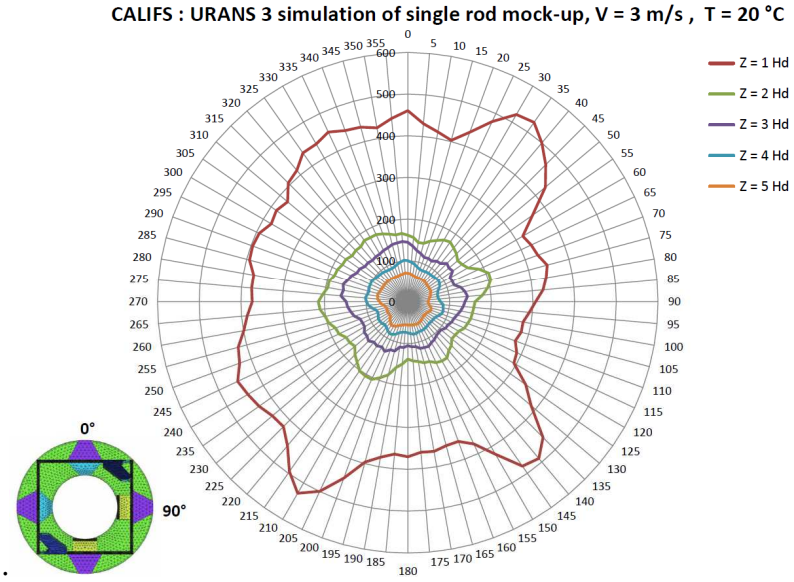

Figure 11 - URANS 3: Azimuthal pressure fluctuation at different levels

The first LES model WALE 1 (Figure 12) gives slightly overestimated fluctuation levels of 10% to 15% at 1 H_d altitude. For the following levels 2 H_d and 3 H_d the values of the maximum fluctuations are correct, and then at the distance of 5 D_h, the level is overestimated by 30%. The angular orientation of the maximums is correctly reproduced at altitude 1 H_d. But for the following levels more elongated azimuthal profiles are observed, the orientation of the maximums of level 2 H_d is shifted by 30° with respect to the measurements. From level 3 H_d we note a rotation of the maxima

of 10° between each level, not observed on the measurements.

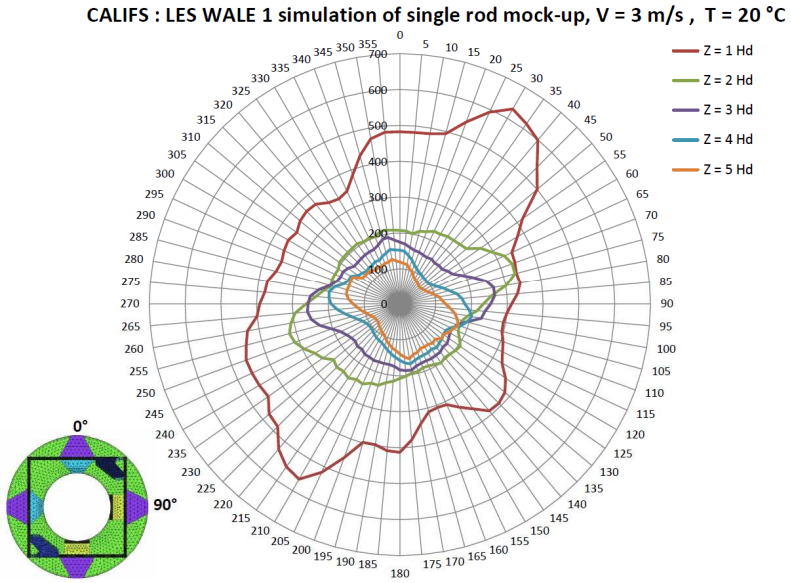

Figure 12 - LES WALE 1: Azimuthal pressure fluctuation at different levels

The second LES model WALE 2 (Figure 13) gives fluctuation levels slightly overestimated from 10% to 15% at altitude 1 H_d. For the following levels 2 H_d and 3 H_d the values of the maximum fluctuations are correct but at 5 D_h the level is still overestimated by 30%. With this new modeling, the angular orientation of the maximums is even better reproduced at the altitude 1 H_d. But at the higher levels we observe (as for the WALE 1 model) a 30° offset of the orientation of the level 2 H_d. and then from 3 H_d the distributions are more elongated than those of the measurements with a rotation of 10° between each level.

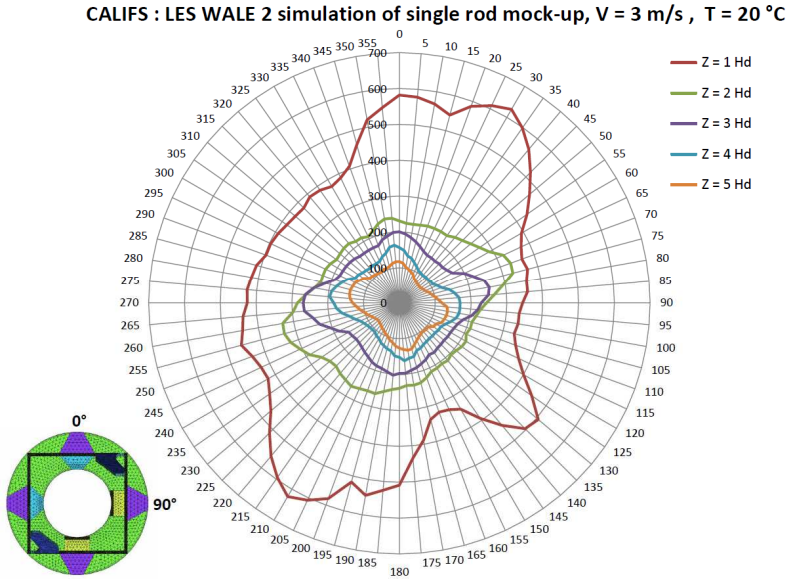

Figure 13 - LES WALE 2: Azimuthal pressure fluctuation at different levels

This first comparison step shows that the URANS models represent rather roughly the azimuthal distribution of the pressure fluctuations: the amplitudes of the maximums are correct at the distance 1 H_d and then underestimated in the following planes. The two LES WALE models yield results whose fluctuation levels are more accurate. The LES WALE 2 model, with the most refined mesh, reproduces more accurately the azimuthal distribution on level 1 H_d as well as the decrease in pressure fluctuations along the rod wall after the grid. However, we observe on both LES models

an orientation shift of 30° of the azimuthal distributions from the level 2 H_d which is not measured experimentally.

It is observed that with identical meshes, the URANS 3 and LES WALE 1 models give very different results, illustrating the greater dependency of the results to the numerical scheme than to the discretization. More generally, the comparisons above show that the LES WALE numerical scheme is less dissipative than the URANS scheme (k-ε).

Note: The transverse velocity cut-views provided at different levels downstream of the grid fins (see section 3.3 - figures. 15 to 17) show reversed coupled swirls. These four swirls create a transverse fluid circulation in the section. These fluid flows create on the rod surface an alternating of close zones where the transverse velocity of fluid changes very rapidly between 0.7 m / s and 0.002 m / s, over short distances. The impact of these velocity fields on the rod surface is at the origin of the azimuthal profiles of pressure fluctuations observed.

The angular offsets of the pressure fluctuation profiles observed between the modeling and the experiment can be partially explained. Indeed for identical locations (axial and azimuthal), the fluctuating pressure values measured are averaged on the rod surface over a diameter of 2 mm, while on numerical models the pressure value is recorded on a single node (closer to the center of the measuring point). This results in a greater sensitivity of the digital probes to the spatial distribution of the pressure fluctuation field at the surface of the rod. The geometric definition of the local digital probes will therefore have to be improved in the next simulations in order to remove the indeterminations that exist in our comparisons.

3.3 Topology of flows and streamlines in the fluid domain

The visualizations of the streamlines and the sections of the velocity field downstream of the mixing grid of the model LES WALE 2 are provided in Figures 14 to 17. They allow a better understanding of the topology of the flow and illustrate the causality of the flow structure on the location and amplitude of the pressure fluctuations observed at the rod wall.

The streamlines (Figure 14), whose colors are associated with the intensity of the fluid velocity, show the deviations and restrictions of section at the grid due to the centering pads, the springs and the dimples in the Grid cell. A maximum velocity of 6.86 m/s is observed locally while the flow rate is 3 m/s. At the output of the mixing grid two phenomena are observed, a general winding of the flow due to the inclination of the two fins and more locally the creation of "swirls" in the respective wake of each mixing vanes.

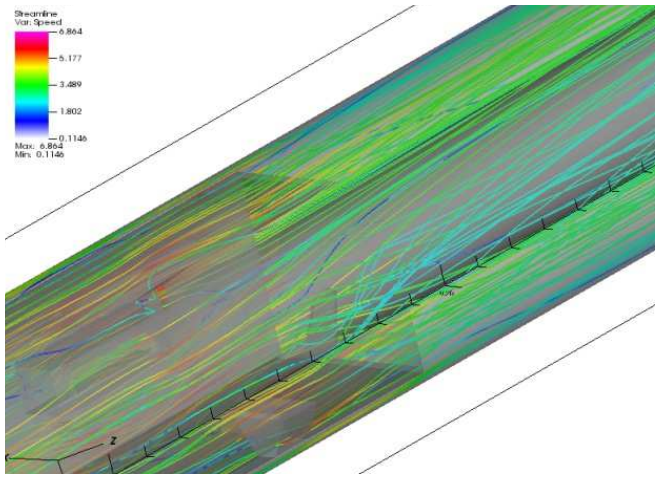

Figure 14 : Flow lines downstream of the mixing vanes

On the figures 15 to 17, the axial and transverse sections provide the azimuthal distribution of the pressure fluctuation maxima depending on the streamlines along the rod downstream of the mixing grid.

- Cutting section at 1 D_h downstream of the grid.

At the bottom of the vanes, Figures 15 (a) and 15 (b) show the appearance of two "swirls" turning in opposite directions, oriented at 30° and 210°. These swirls have transverse rotation speeds around 1.2 m/s and locally the axial velocity reaches 4.6 m/s The jet effect is visible at 135° and 315° due to the restrictions in the grid section, the jets at 45° and 225° being disturbed by the effect of the fins. These complex fluid movements explain the origin of the irregular distributions of the pressure fluctuations observed in different planes at the rod wall downstream of the grid (see Figure 8).

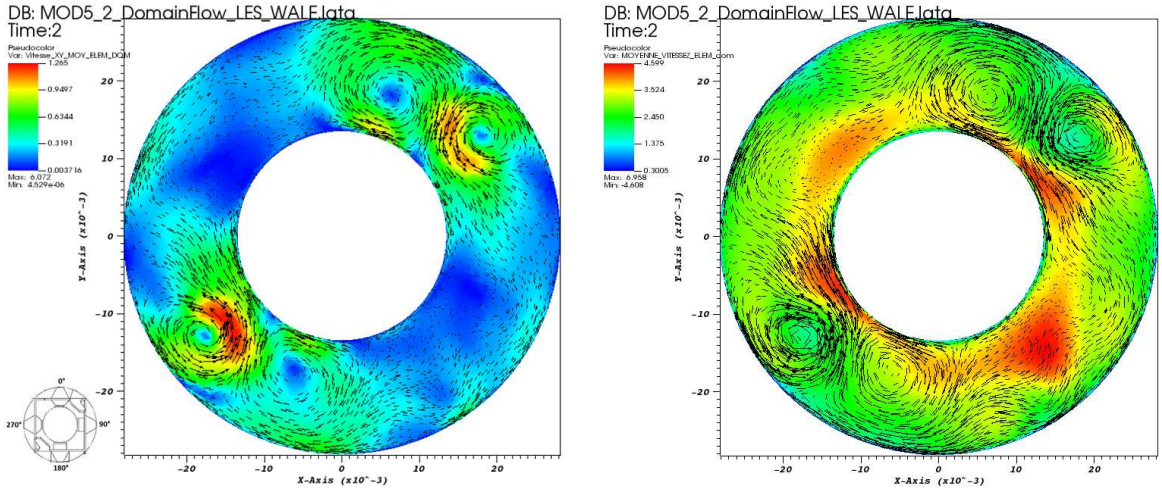

(a) Cross sectional velocity (b) Axial velocity

Figure 15 : Axial and transverse average speeds 1 H_d downstream of the mixing grid

- Cutting section at 2 H_d downstream of the grid.

At two hydraulic diameters (Figure 16) the jet effect decreases (from 4.6 m/s to 4.14 m/s). The jets at 45° and 225° are still hidden by the swirls. The speed of rotation of the swirls decreases by a factor of 2 (from 1.2 m/s to 0.7 m/s). The symmetry axes of the swirls are now oriented at 40° and 220°, they have moved about is approximately 10° in the reverse trigonometric direction.

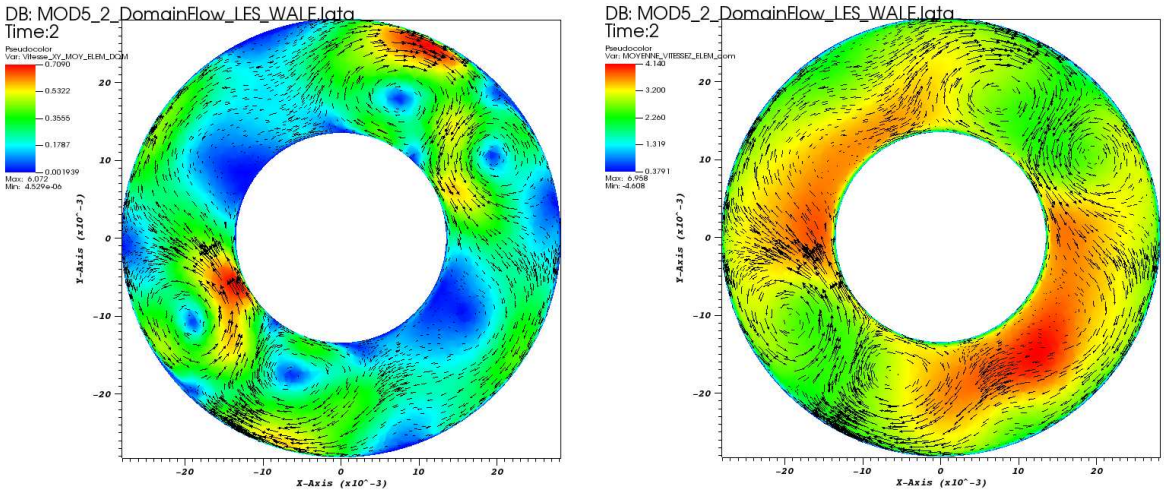

(a) Cross sectional velocity (b) Axial velocity

Figure 16 : Axial and transverse average speeds 2 H_d downstream of the mixing grid

- Cutting section at 5 H_d downstream of the grid.

At the level 5 H_d downstream of the grid, the axial velocity field is now almost homogeneous over the entire circumference (Figure 17 (b)), the maximum axial velocity decreased to 3.47 m/s,

which is close to the maximum speed profile in the section before the grid. Considering transverse flows (Figure 17 (a)), we note that the vortices have almost completely disappeared in favor of a "square" circulation around the rod.

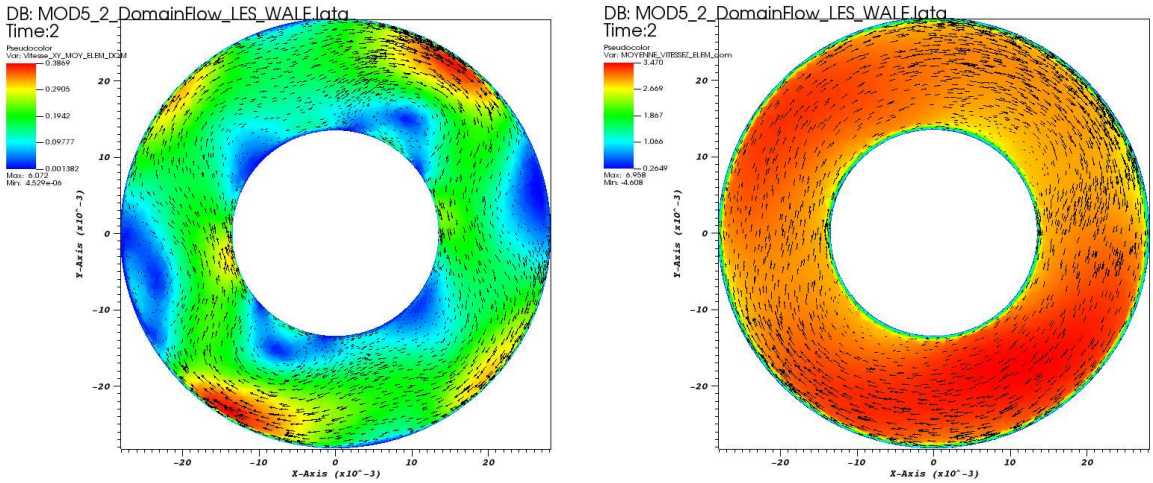

(a) Cross sectional velocity (b) Axial velocity

Figure 17 : Axial and transverse average speeds 10 H_d after mixing grid

Beyond 10 H_d, the decrease of the transverse velocity is correlated with the homogenization of the profile of the axial velocity in the whole section. The distribution of the azimuth pressure fluctuations becomes more uniform with a standard deviation equivalent to that observed upstream of the grid.

3.4 Comparison between computational and experimental spectra of local pressure fluctuations

This paragraph presents the comparison between the PSD spectra resulting from measured and simulated local pressure fluctuations of the LES WALE 2 model, since it proves the most promising for the continuation of the current work.

To observe the impact of the choice of inlet conditions for identical models, we present here the results of two variants of the LES WALE 2 simulation. In the first case, the inlet conditions of the fluid at the entry of the studied domain are generated at each time step by using a recirculation box according to the methodology described previously in this article. Then a second calculation was carried out with the same mesh and the same digital patterns but by this time applying to the inlet of the domain a constant average speed profile obtained at the outlet of the periodic box.

- LES WALE 2 model - Calculation coupled with the periodic box

The most significant PSD spectra of the LES WALE 2 modeling yield the following observations.

- In the plane located 1 H_d downstream of the grid, compared spectra in the wake of the vanes at 40° (Figure 18) and 210° (Figure 19) show a change of slope around 100 Hz. The frequency peaks are reproduced with a frequency offset of 4 Hz at 5 Hz and with a magnitude overestimated by a factor 4 at azimuth 210°.

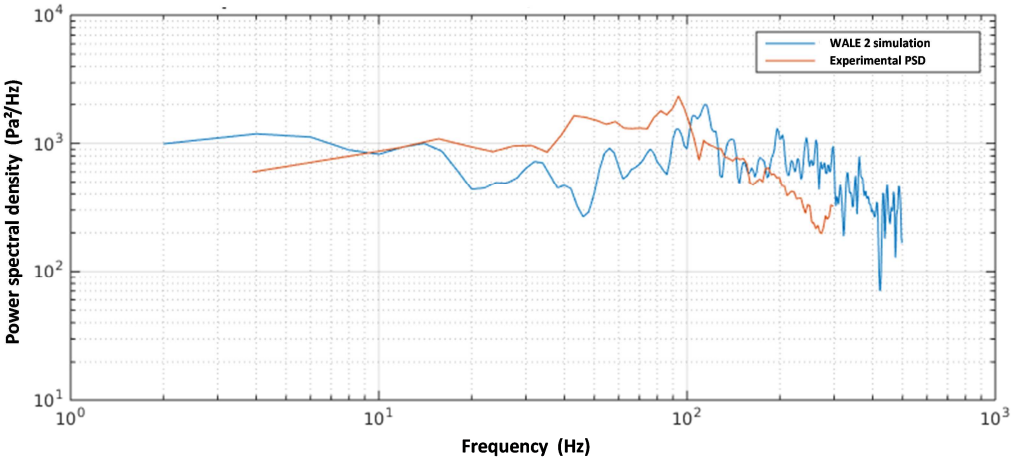

Figure 18 – LES WALE 2 model - Comparison of PSD between simulations and experience (1 H_d, azimuth 40°)

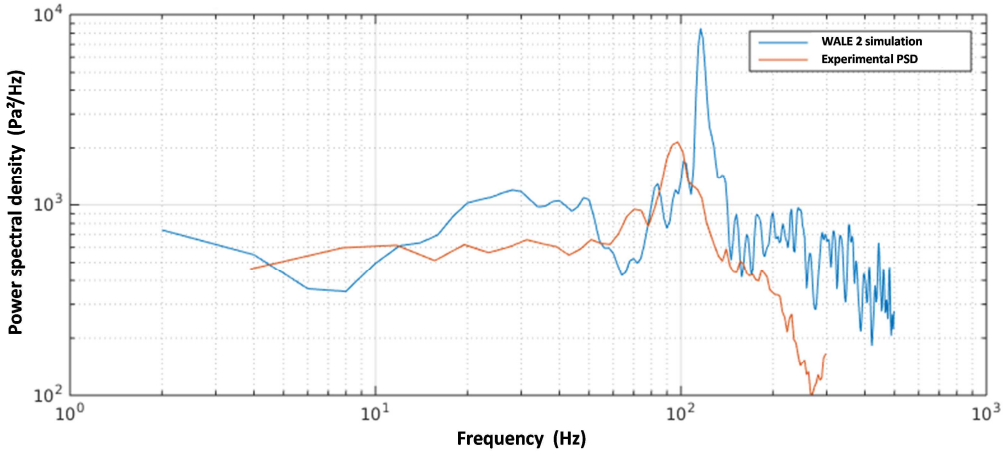

Figure 19 – LES WALE 2 model - Comparison of PSD between simulations and experience (1 H_d, azimuth 210°)

- In the plane located at 2 H_d downstream of the grid (Figures 20 and 21) the spectra show good agreement, the calculated and experimental slopes being of the same order of magnitude with still a slight frequency offset.

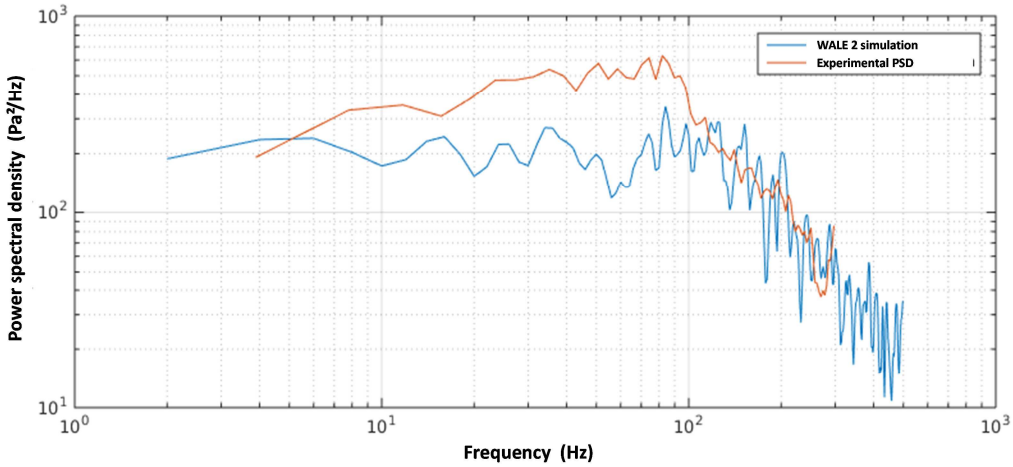

Figure 20 – LES WALE 2 model - Comparison of PSD between simulations and experience (2 H_d, azimuth 40°)

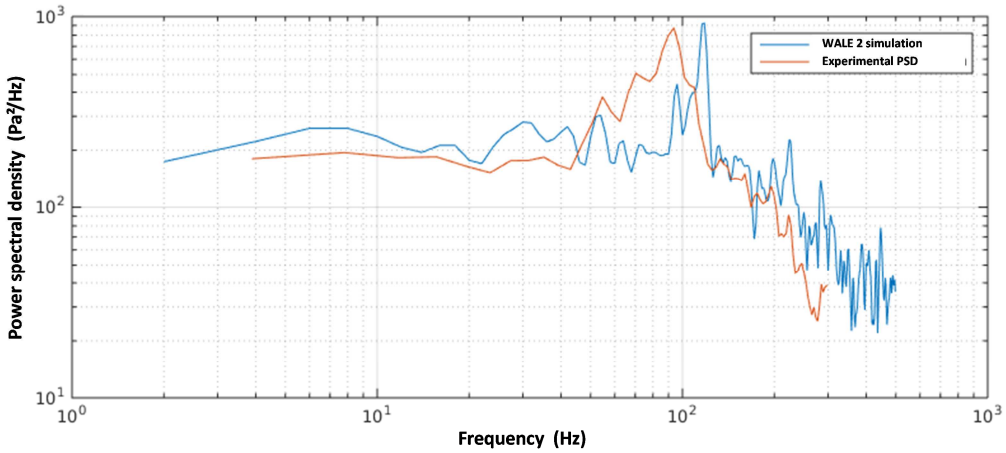

Figure 21 – LES WALE 2 model - Comparison of PSD between simulations and experience (2 H_d, azimuth 210°)

As before, these comparisons must be put in perspective because of the difference between the experimental probes giving spatially averaged pressure values over a diameter of 2 mm and the modeled probes giving a value in a single node, the latter being therefore more sensitive to local effects of turbulent fluctuations due to swirls. The comparison shows nevertheless a realistic reproduction of the bandwidth and frequency peaks.

More generally, as one moves away from the grid, the flow stabilizes and the turbulent intensity decreases, the effect of which is to mitigate the differences between the experimental and calculated PSD spectra.

- LES WALE 2 model - Constant input speed profile without periodic box

The DSP spectra of the LES WALE 2 calculation, showing a constant velocity profile at the inlet of the studied domain, give very different results from those obtained with the same model coupled with the periodic box.

- In the plane distant 1 H_d downstream of the grid (Figures 22 and 23), the comparison with the DSP measurements of the probes located in the wake of the fins at 40° and 210° reveals a significant deficient levels of pressure fluctuations at low frequency in the range between 3 Hz and 100 Hz. Frequency peaks are observed around 200 Hz, this 100 Hz offset from the measurements is much greater than in the previous calculation (Figures 18 and 19).

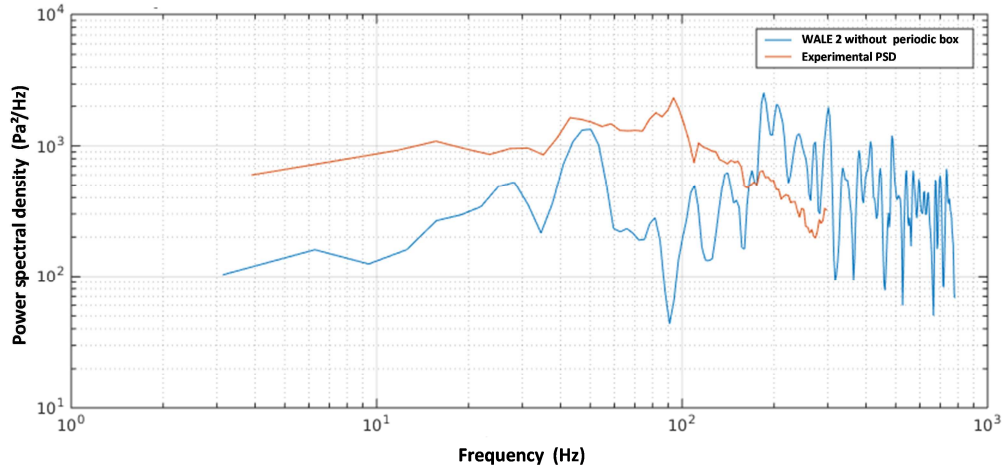

Figure 22 – LES WALE 2 model without periodic box - Comparison of PSD between simulations and experience (1 H_d, azimuth 40°)

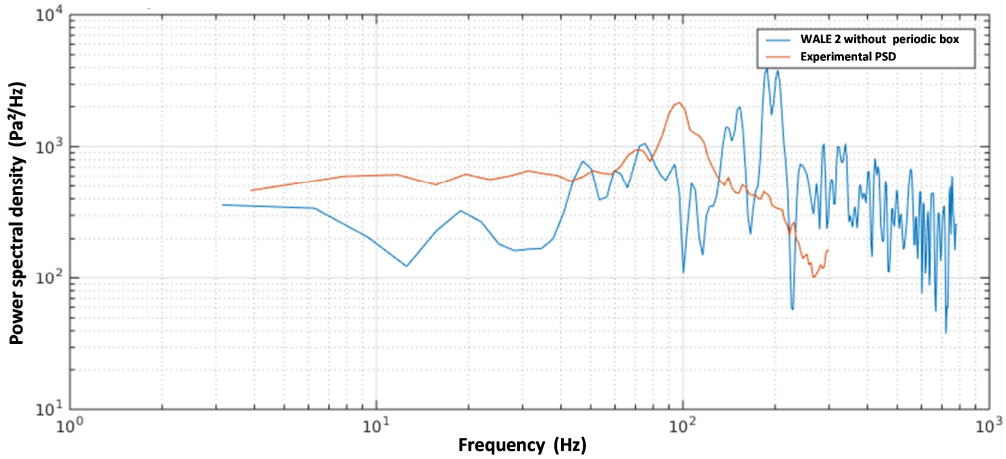

Figure 23 – LES WALE 2 model without periodic box - Comparison of PSD between simulations and experience (1 H_d, azimuth 210°)

- In the plane distant of 2 H_d downstream of the grid (Figures 24 and 25), we observe again low levels in the frequency range between 3 Hz and 100 Hz and the frequency peaks shifted by 100 Hz by comparing with fluctuating pressure measurements is greater than in previous calculation (Figures 20 and 21).

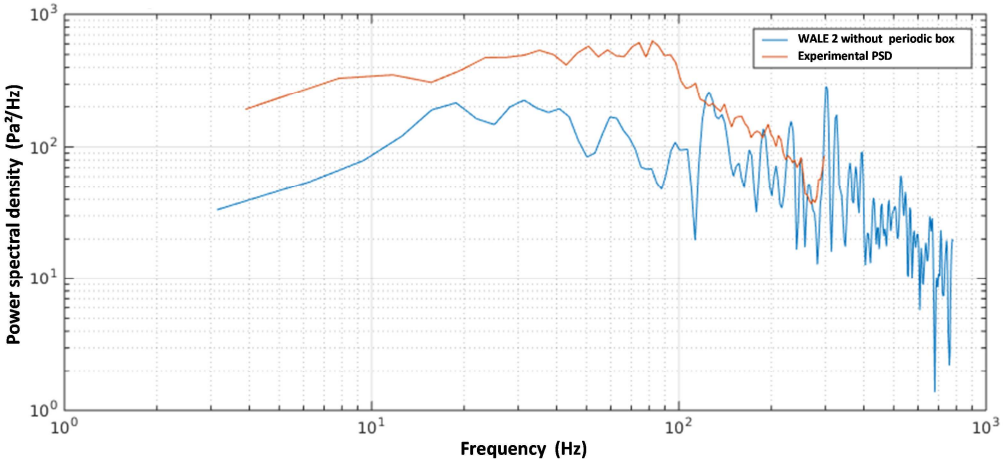

Figure 24 – WALE 2 model without periodic box - Comparison of PSD between simulations and experience (2 H_d, azimuth 40°)

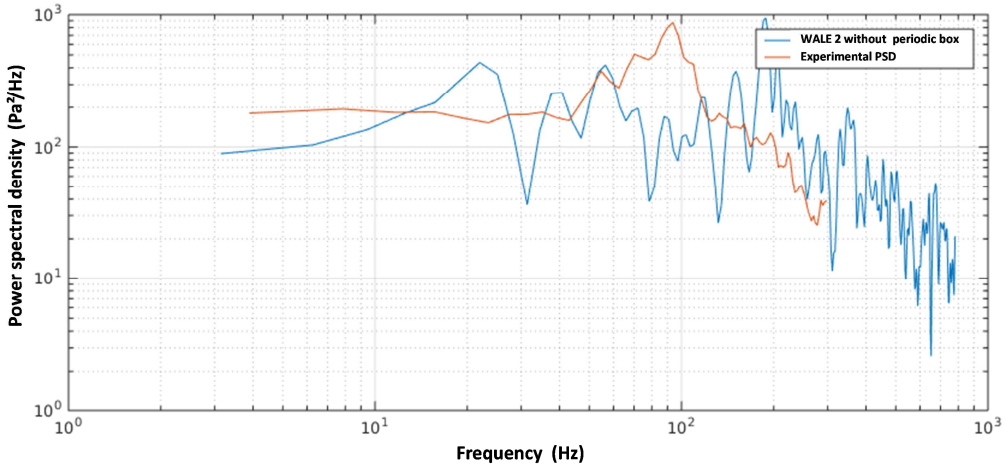

Figure 25 – WALE 2 model without periodic box - Comparison of PSD between simulations and experience (2 H_d, azimuth 210°)

Similar results are observed on all the 360 point probes of the LES WALE 2 model placed in the 10 measurement planes downstream of the grid. The influence of the inlet conditions was tested identically on the LES WALE 1 model. Here again, the calculation using the instantaneous speed profile (updated at each time step) at the inlet of the domain gives the closest results to the experimental results.

This additional comparison allows us to validate aspects of the study concerning the generation of the inlet conditions of the fluid in the control volume.

3.5 Spectral analysis of the fluctuating forces integrated on the wall of the rod

Since the measurements of the force fluctuation spectra at the wall are not directly accessible, the validation of the numerical models is primarily made, as we have just seen, by comparing the results of the modelizations with local measurements. However the objective of our modeling remains the determination of the spectra of the resultant of the pressure force fluctuations onto the wall integrated along the axis of the rods.

With the simplified geometry used in the present study, it is only possible to perform qualitative comparisons with the FIX spectra [18] and the internal flow spectra from Clinch [19] and Axisa [20] (see Figures 26 to 28), with numerical results from the LES WALE 2 case). In order to simplify the comparisons and the reading of the curves, the maximum amplitude of the internal flow spectrum (Clinch, Axisa) has been recalibrated on that of the tube bundle spectrum (FIX) while preserving the slopes and frequencies of the inflection points of each curve. This recalibration is carried out by applying a multiplier coefficient on the coefficient "a" of the spectrum of (Clinch, Axisa).

Since the flow is confined in an annular space, the simulated spectra show similarities with the two families of reference spectra:

- a frequency bandwidth with a point of inflection at the reduced frequency fr = 1, similar to that of an internal flow in a pipe,
- a slope of -3/2 for a reduced frequency fr $\geq$ 1 , similar to that of a flow in a rod bundle.

The fluctuations in the spectra of the resulting transverse pressure forces decrease very rapidly after 6 H_d, which results in a decline in the overall level of the amplitude but the width of the frequency band remains almost constant.

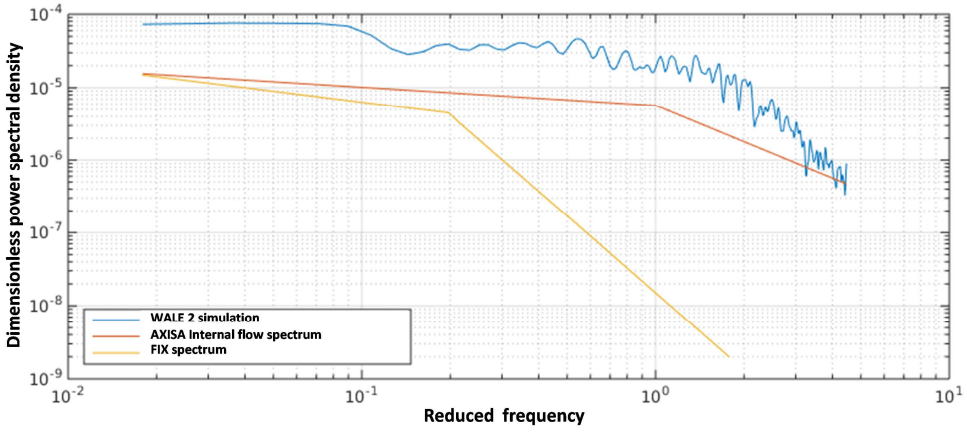

Figure 26 – LES WALE 2 model - PSD of the resulting dimensionless pressure force at 0.2 H_d downstream of the grid

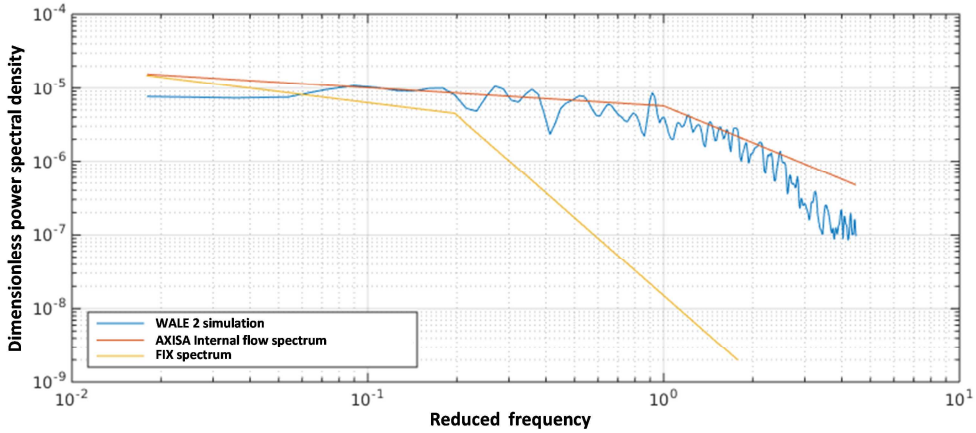

Figure 27 - LES WALE 2 model - PSD of the resulting dimensionless pressure force at 3 H_d downstream of the grid

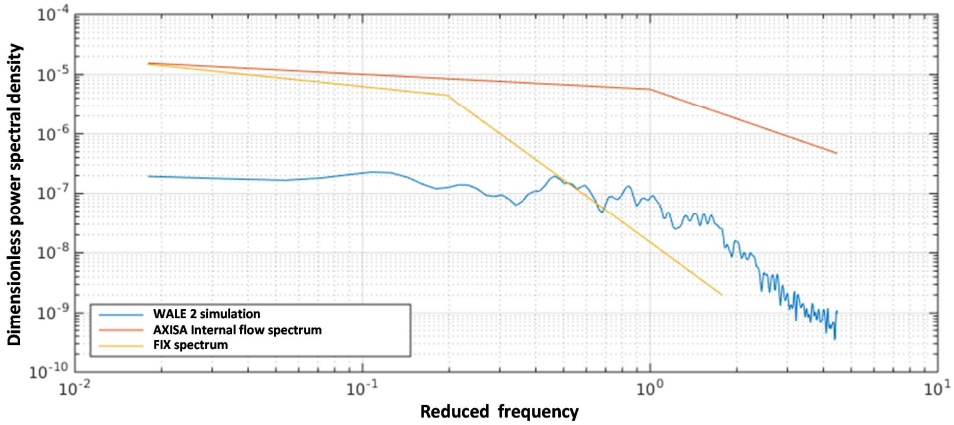

Figure 28 - LES WALE 2 model - PSD of the resulting dimensionless pressure force at 13 H_d downstream of the grid

To conclude this section, the overall analysis of the 41 spectra for each of the 5 proposed simulations cases (which cannot be all displayed in the present paper), show that:

- the approach by spatial integration of the pressure forces components is relevant to visualize spectra and compare them to theoretical results,
- the LES WALE 2 model provides again the most accurate spectral content with respect to the reference dimensionless spectra.

3.6 Decreasing of turbulent energy

It clearly appears on the plot of standard deviation of the transverse pressure force drawn along the rod (Figure 29), that the two kinds of turbulence models used in the simulation produce two families of curves independently from the mesh (let us remind here that the models URANS 3 and LES WALE 1 share the same mesh).

We observe that:

- for models URANS 1, 2 & 3 :
  - amplitudes of forces fluctuations comparable for the 3 URANS models,
  - decay is similar for the 3 meshes,
  - turbulence levels are overestimated after the grid and then a faster dissipation on the rod height a for the 3 modeling URANS.
- for models LES WALE 1 & 2 :
  - on the modeling WALE 1 model (y^+=50): the force decay is regular between 0.2 H_d

and 13.5 H_d, and the resulting forces exerted on the rod after the grid are lower than for the URANS models,

- on the modeling WALE 2 (y^+=32): one notices two inflection points at 2 H_d and 5,5 H_d, it is also noted that just after the grid, the level of the resulting forces exerted on the rod is intermediate between the URANS And WALE 1,
- for these two LES models, the dissipation is less important along the rod compared to the 3 URANS models.

Based on the experimental data available at the time of the study and taking into account the results of previous comparisons, the LES WALE numerical model seems to correspond best with the needs of the next modeling of the 5x5 rods assembly mockup (see the perspectives in Section 4). Considering the singularities observed on the model WALE 2, the mesh will have to be refined from inside the grid and up to a distance of 6 H_d Dh downstream of it.

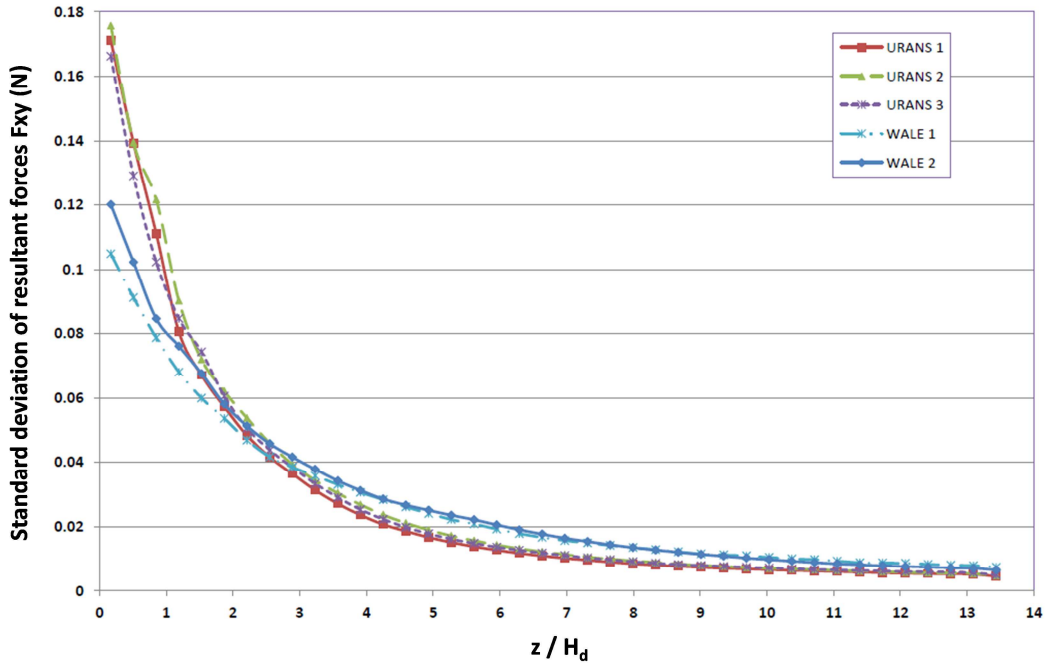

Figure 29 : Resultant of the wall-forces integrated along the rod between 0.2 and 13.5 H_d

4. Summary

The cross-comparisons of the results of the simulations with the measurements carried out on the single-rod calibration bench focused on several criteria :

- the respect of the axial velocity profiles in an annular canal,
- the reproducibility of the order of magnitude and the azimuthal distribution of the pressure fluctuations at the wall,
- the quality of the comparisons of the simulated spectra with the measurements of pressure fluctuations at the wall,
- the comparison of the integrated force spectra at the wall with the experimental reference spectra and the literature, despite the limitations due to differences in the geometries considered,
- the decay of the turbulent energy associated with the decay of the fluctuating forces at the wall over the height of the rod.

The analysis shows that the LES WALE turbulence model better captures the physics of the

flow. It is most promising for future modeling of CALIFS test experiments with 5x5 rod bundle configuration.

Nevertheless, despite the differences observed in the simulated fluctuating pressures with the different models, resulting forces along the rod relatively close to the experiment are obtained in all cases between 1 and 13 H_d downstream of the mixing grid. This shows that a prediction of fluctuating forces by 3D numerical modeling methods in fluid mechanics is accessible and robust.

5. Future work

The experimental CALIFS tests carried out in 2016 on the two models of 5x5 rods assemblies equipped with grids with (or without) mixing vanes provide a complete experimental database combining measurements of pressure fluctuations wall of the rods and complete measurements of velocities by LDV in the fluid [1].

The simulation of the 5x5 bundle model equipped with grids without mixing fins over a total height of 25 H_d. is in progress. The two configurations are presented hereafter, a partial mesh around the central rod with lateral periodicity conditions at the vertical cutting section of the adjacent rods and the complete model of the mockup.

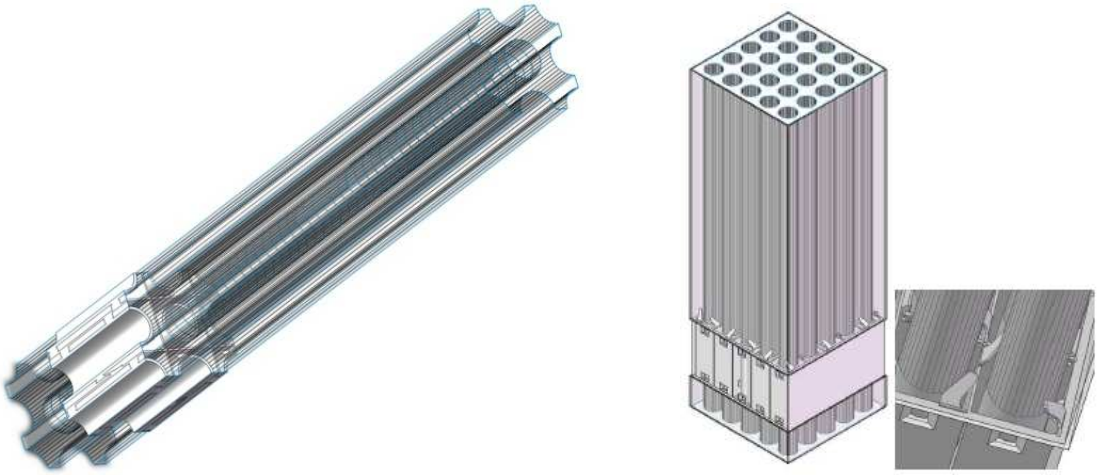

(a) Partial model with lateral periodicity boundaries

(b) Complete model 5x5 rods

Figure 30 : Configurations simulated in 2016

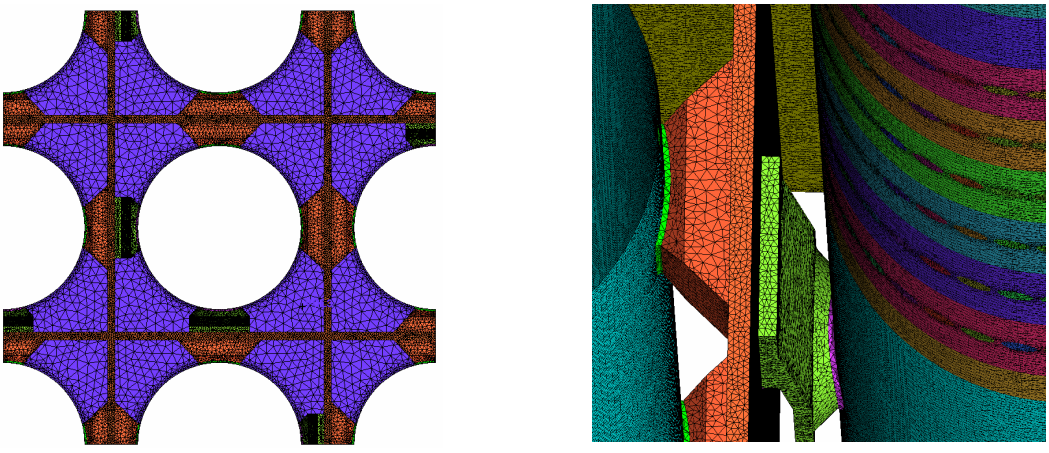

(a) Top view

(b) Detail of support springs

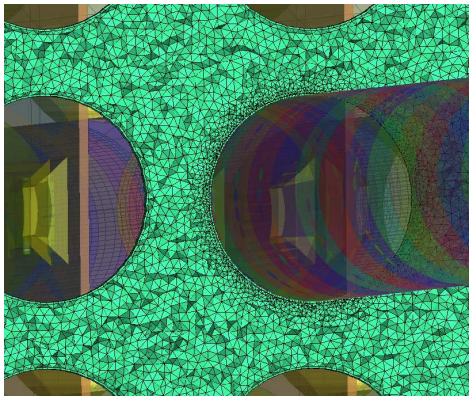

(c) Model 5x5 rods - Mesh seen from above

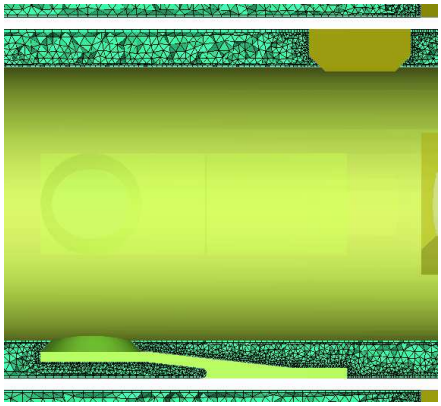

(d) Detail of the mesh of springs and dimples

Figure 31 : Meshes of partial model (3x3) and complete model (5x5)

The objectives of the real geometry modeling are :

- the estimation of the singular and regular pressure losses,
- the study of the spatial and temporal coherence lengths thanks to a better geometric definition of the point probes for comparison with the measurements,
- the determination of the turbulent energy decay,
- the determination of the integral scale of turbulence length and then of the turbulent energy spectra as a function of the wave number,
- the realistic determination of the vibratory excitation forces on the walls of the fuel rods.

This next step should allow an in-depth comparison with the reference experiment and help to validate the use of CFD simulations for the estimation of the fluctuating fluid forces exerted at strong Reynolds on the fuel rod bundles.

Acknowledgments

I thank Francis Moreno of the CEA of Cadarache for the quality of his work, the reliability of the measures provided and his availability. My thanks go also to the development team of the TrioCFD code of the CEA of Saclay, in particular to Ulrich Bieder and Gauthier Fauchet for their advice on the implementation of the digital schemes as well as to Céline Capitaine of TrioCFD technical support. I would also like to thank the successive project managers, Bruno Collard and Vincent Faucher, who supported this project with our industrial partners and with the commissions allocating the calculation resources of the TGCC.

References

[1] Measurement of fluctuating fluid pressure exerted on the wall of tube buddle Francis Moreno, Bruno Collard, Vincent Faucher, FIV 2016 11th Conference on Flow-Induced Vibration and Noise The Hague, The Netherlands, 4-6 July 2016.

[2] Time domain modelling of the random vibrations of tubes subjected to turbulence conveying flows, ASME Pressure Vessel and Piping Conference (PVP-2011), Baltimore.

[3] Identification of random excitation fields from vibratory responses with application to multi-supported tubes excited by flow turbulence J. Antunes, L. Borsoi, X. Delaune, P. Piteau, ASME Journal of Pressure Vessel Technology (2014).

[4] Base de validation du logiciel TrioCFD - Guide des bonnes pratiques. S. Vandroux, V. Barthel. DEN/DANS/DM2S/STMF/LMSF/NT/13-008/A.

[5] Vollstaendige Dartellung der turbulenten Geschwindigkeitsverteilung in glatten Leitungen, H. Reichardt, Z. Angew. Math. Mech, 31(7), 1951, pp. 208-219.

[6] High-resolution FEM-TVD schemes based on a fully multidimensional flux limiter. D. Kuzmin, S. Turek. Journal of Computational Physics, Volume 198, Issue 1, 20 July 2004, pp.131–158.

[7] The numerical computation of turbulent flows. B.E. Launder, D.B. Spalding. Computer Methods in Applied Mechanics and Engineering. March 1974 3 (2): pp. 269–289.

[8] B.E. Launder, G.J. Reece, W. Rodi. Progress in the development of a Reynolds- stress turbulence closure. I. Fluid Mech. 68:537-66, 1975.

[9] Subgrid-scale stress modelling based on the square of the velocity gradient tensor. Flow, F. Ducros and F. Nicoud, Turbulence and Combustion, Vol. 62, Number 3, 183-200, 1999.

[10] General circulation expériments with the primitive equations. S. Smagorinsky, Mon.Weather, vol, 91, 1963, pp.99-164.

[11] A proposed modification of the germano subgrid-scale closure method. D.K. LILLY. Physics of Fluids, Vol. A 4(3), 1992.

[12] Numerical simulation of developing and decaying two-dimensional turbulence, D. K. LILLY, Journal of Fluid Mechanics, Vol. 45, Issue 02, January 1971, pp 395- 415.

[13] Développements et validation de simulation des grandes échelles d'écoulements turbulents dans un code industriel, C. ACKERMANN, Thèse CEA Grenoble, 22/12/2000.

[14] Méthodes et techniques de traitement du signal et applications aux mesures physiques, J. Max; L. Audaire, D. Berthier, R. Bigret, (et al.) Editions Masson 1987.

[15] Matlab, Signal Processing Toolbox, User's Guide.

[16] Flow of Newtonian and non-Newtonian fluids in concentric and eccentric annuli, J. M. Nouri, H Umur, J. H. Whitelaw, J. Fluid Mech. (1993), vol. 253, pp 617-641.

[17] Direct numerical simulation of turbulent concentric annular pipe flow, Part 1 : Flow field, S. Y. Chung, G. H. Rhee, H. J. Sung, International Journal of Heat and Fluid Flow 23 (2002), pp 426-440.

[18] Maquette FIX : Auto spectre adimensionnels des efforts fluctuant – B. BEAUFILS, J. PORTIER (1991) – Rapport CEA/DMT/91/615.

[19] Measurements of wall pressure field at the surface of smooth-walled pipe containing turbulent water flow, J. M. CLINCH, J. of Sound and Vibration, Vol. 9, p.398-419, 1969.

[20] F. Axisa, Vibrations sous écoulement. Hermes Science Publications, Paris (2001).